ACS Sustainable Chemistry & Engineering

Research Article

pubs.acs.org/journal/ascecg

Valorization of Lignin Waste: Carbons from Hydrothermal Carbonization of Renewable Lignin as Superior Sorbents for CO_2 and Hydrogen Storage

Wantana Sangchoom and Robert Mokaya*

University of Nottingham, University Park, Nottingham NG7 2RD, United Kingdom

Supporting Information

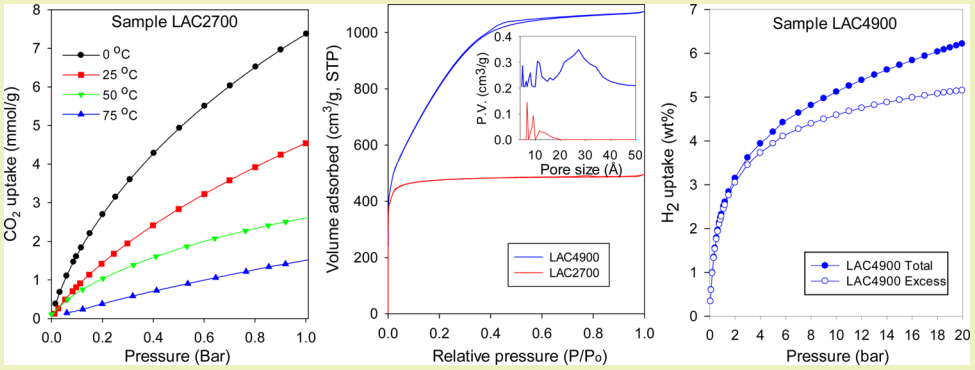

ABSTRACT: This report presents the preparation of renewable carbons from hydrothermally carbonized lignin waste. The hydrothermally carbonized mineral-free lignin-derived hydrochar was activated with KOH to yield carbons with surface area of 1157−3235 m^2 g^{-1} and pore volume of 0.59−1.77 cm^3 g^{-1}. Activation at KOH/carbon = 2, generates highly microporous carbons (≥97% micropore surface area and 93% micropore volume), which exhibit excellent CO_2 uptake capacity; up to 4.6 mmol g^{-1} at 1 bar and 25 °C, and 17.3 mmol g^{-1} at 20 bar and 25 °C, whereas at 0 °C and 1 bar, they store up to 7.4 mmol g^{-1}. Activation at KOH/carbon = 4 can generate carbons with surface area and pore volume of up to 3235 m^2 g^{-1} and 1.77 cm^3 g^{-1}, respectively, which have hydrogen uptake of up to 6.2 wt % at −196 °C and 20 bar. The simplicity of hydrothermal carbonization in generating hydrochars suitable for activation from readily available lignin waste, without the need for a demineralization step, makes these carbons attractive as gas storage materials for energy related applications. Furthermore, the lignin-derived carbons offer advantages with respect to attainable porosity and gas storage capacity compared to other forms of biomass (e.g., cellulose)-derived carbons.

KEYWORDS: *Lignin hydrochar, Hydrothermal carbonization, CO_2 capture, Hydrogen storage, Activated carbon, Lignin waste, Activation, Biomass*

INTRODUCTION

Currently, storage of energy related gases in porous materials is attracting a great deal of attention due to ever increasing demands for new, efficient and clean energy sources as best illustrated by the need for CO_2 sequestration and the drive toward the Hydrogen Economy.[1−6] The ongoing search for suitable porous solids that are able to store large amounts of CO_2 and hydrogen is one of the most active research areas in energy materials chemistry.[7−28] The development of solid state adsorbents that can efficiently store hydrogen or sequester polluting greenhouse gases such as CO_2 would certainly convey economic and environmental benefits and contribute to reduction in our reliance on fossil fuels.[1−28] Thus, with regard to the increasing number of possible energy related applications, new synthesis methods are intensively being developed to generate new and optimized porous materials for specific applications. For gas storage applications, new porous materials should possess the appropriate porosity;[8−16] it is known that the adsorption capacity of porous materials depends strongly on surface area and pore structure.[8−16] Among porous materials, activated carbons have attracted a lot of interest due to their ease of preparation, variable pore structure, good chemical stability and tunable pore size.[12] Furthermore, activated carbons may be prepared from a variety of raw materials, and variation of synthesis conditions may be used to control the pore structure and consequently optimize gas sorption/storage capacity.[12]

Recently, we and others have reported that activated carbons derived from polymers or biomass show high hydrogen and CO_2 storage capacity.[21,25−27,29−31] Traditionally, activated carbons may be prepared by two types of activation

Received: April 24, 2015
Published: June 4, 2015

DOI: 10.1021/acssuschemeng.5b00351
ACS Sustainable Chem. Eng. 2015, 3, 1658−1667

approaches: physical and chemical activation. Activation of carbon precursors via physical activation occurs via gasification wherein oxidizing gases such as CO_2, steam or air are employed. In chemical activation, the precursors are mixed with chemical activating agents such as KOH, NaOH or $ZnCl_2$ etc., and then subjected to heat treatment in inert atmosphere at various temperatures.[12] In the search of porous carbons suitable for hydrogen and CO_2 storage, it would seem highly desirable to employ new types of sustainable and renewable precursors that may lead to novel sorbents with excellent storage capacity. Hydrothermal carbonization is an attractive method for generating low-cost and environmentally friendly carbons from natural materials.[32] Although the traditional production of char via dry pyrolysis takes place in the absence of oxygen via processes that increase the carbon content,[33] hydrothermal carbonization, on the other hand, involves the thermochemical decomposition of biomass in the presence of water to generate products (namely hydrochar) with a higher carbon content,[32,34] and which may be used as a precursor in activated carbon production.

Lignin is the second most abundant natural and renewable raw material after cellulose, and is present in plants as the glue that holds together cellulose fibers. Extraction of cellulose, which is considered to be a higher value material, and cellulose-based products requires the removal of lignin from plant-based raw materials. The cellulose extraction process generates large amounts of low value residue (waste) whose main component is lignin. The disposal of such lignin-based residue, especially the waste that is generated as so-called black liquor by the pulping industry during the manufacture of paper, can be cause for environmental concerns. Much of the lignin waste, as black liquor, is used as an energy source in the pulping industry due in part to the fact that unlike other types of biomass that can be converted into higher value chemicals, lignin is the only large volume renewable feedstock that comprises aromatics, which means that there are still no routes for its valorization to single aromatic feedstocks.[35] It is therefore desirable to find other avenues of converting lignin waste into higher value materials. A good example is use of lignin as a precursor for activated carbon.[36] However, prior to activation, the lignin is typically pretreated (i.e., demineralized) to remove mineral matter,[36] which requires the undesirable use of acid or alkali. Indeed, to date, the preparation of activated carbons from lignin typically incorporates a demineralization step.[36] Moreover, as far as we know, and despite the large number of studies on hydrothermal carbonization of a variety of biomass sources,[32,34] there are no reports on the hydrothermal conversion of lignin (or lignin waste) to hydrochar.

In this report, therefore, we explore the hydrothermal carbonization of lignin waste as a means of enriching the carbon prior to activation, and seek to find out whether such carbonization can replace the demineralization step. We have used hydrochar that is derived from hydrothermal carbonization of lignin waste as a precursor for activated carbons. Although several studies have already shown that activation of hydrochar generated from hydrothermal treatment of biomass yields activated carbons that exhibit attractive porosity,[12] lignin presents an interesting case with respect to activation due to its apparent low reactivity;[35] previous studies have suggested that it is easier to activate carbon with a high cellulose content than that having high lignin content[37,38] and that lignin has low reactivity compared to other biomass-derived carbon due to its highly cross-linked nature.[37] We therefore also offer a discussion on the relative ease of activation of lignin compared to cellulose. The present work used KOH as an activating agent in the temperature range 600−900 °C, and the KOH/carbon ratio was varied so as to generate optimized carbon materials with enhanced CO_2 or hydrogen storage capacity.

EXPERIMENTAL SECTION

Carbon Synthesis. Lignin waste (Borregaard LignoTech) was converted to carbonaceous material (so-called hydrochar) via hydrothermal treatment in high temperature water (300−390 °C). The lignin-derived hydrochar (designated as LD hydrocar) was transformed to activated carbon as follows; the dry hydrochar was thoroughly mixed with KOH in an agate mortar at a KOH/carbon ratio of 2 or 4. The mixture was placed in an alumina boat and heated (at heating ramp rate of 3 °C min^{-1}) in a horizontal furnace under nitrogen flow at activation temperatures ranging from 600 to 900 °C for 1 h. Once the sample was cooled down under nitrogen flow, the resulting carbon was washed several times with 1 M HCl at room temperature and then washed with sufficient distilled water until neutral pH. Finally, the carbon was dried at 120 °C for 3 h. The lignin-derived activated carbons were denoted as LACxT where x is the KOH/carbon weight ratio (2 or 4) and T is the activation temperature (°C).

MATERIAL CHARACTERIZATION

Nitrogen sorption isotherms and textural properties were measured at −196 °C using nitrogen in a conventional volumetric technique by a Micrometrics ASAP 2020 volumetric sorptometer. The activated carbons were outgassed under vacuum at 200 °C for 12 h before analysis. The surface area was calculated using the BET equation applied to adsorption data in the relative pressure (P/P_o) range of 0.02−0.25, and total pore volume was calculated from the amount of nitrogen adsorbed at relative pressure (P/P_0) of 0.99. The micropore surface area and micropore volume were estimated by t-plot analysis. The pore size distributions were obtained via a nonlocal density function theory (NLDFT) method using nitrogen adsorption data. Thermogravimetric analysis was carried out in alumina pans using a TA Instruments SDT Q600 analyzer with heating rate of 10 °C/min to 1000 °C under flowing (100 mL min^{-1}) air or nitrogen conditions. Powder XRD analysis was performed on a Bruker D8 Advance powder diffractometer using Cu Kα radiation (λ = 1.5406 Å) and operating at 40 kV and 40 mA, with 0.02° step size and 2 s step time.

Gas Uptake Measurements. CO_2 uptake measurements were performed on a Hiden intelligent gravimetric analyzer (IGA-003), which has a pressure range of 0−20 bar. Before analysis, the carbon samples were outgassed overnight under vacuum at 250 °C. Then the CO_2 uptake isotherms were obtained at a variety of temperatures between 0 and 75 °C in the pressure range 0−20 bar. CO_2 uptake was also measured using a TA Instruments SDT Q600 analyzer at atmospheric pressure (1 bar). Prior to uptake measurements, the carbon samples were heated to 250 °C under static nitrogen and then cooled to 25 °C under a flow of nitrogen. The samples were then purged with CO_2 (50 mL min^{-1}) for 3 h. Between measurements, desorption of CO_2 was undertaken by heating the sample to 250 °C under nitrogen gas flowing at the rate of 100 mL min^{-1}.

Hydrogen uptake measurements were performed using high-purity hydrogen (99.9999%) over the pressure range of 0−20 bar with an intelligent gravimetric analyzer (IGA-003 Hiden). The samples were outgassed under vacuum at 200 °C overnight before analysis. Then the hydrogen uptake isotherms were

DOI: 10.1021/acssuschemeng.5b00351
ACS Sustainable Chem. Eng. 2015, 3, 1658−1667

measured at −196 °C (under a liquid nitrogen bath). The hydrogen uptake was corrected for buoyancy effect as previously described.[29]

RESULTS AND DISCUSSION

Hydrothermal Carbonization of Lignin Waste. To monitor the changes in the carbon content and the "carbonizing/demineralization" effects of the hydrothermal treatment, we performed thermogravimetric analysis (TGA) of the waste lignin and carbonaceous material (designated as LD hydrochar) obtained from hydrothermal carbonization of lignin waste. The TGA curves are shown in Figure 1. We first note that the TGA

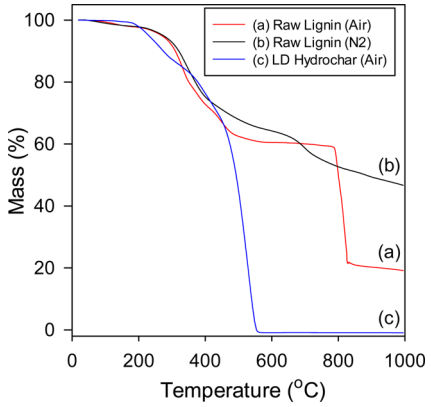

Figure 1. Thermogravimetric analysis curves of raw waste lignin and LD hydrochar obtained from hydrothermal carbonization of the lignin.

curve of the lignin waste under nitrogen indicates a slow volatilization process with a residue of ca. 46% of nonvolatilized matter at 1000 °C, which is similar to what has previously been observed for lignin.[38−41] It has previously been observed that when heated under inert conditions, 40−50 wt % of lignin matter remains nonvolatilized at 800 °C due to the formation of highly condensed aromatic structures.[38−41] Such highly condensed aromatic structures are likely to form char when the lignin is heated under oxidizing conditions. Indeed, as shown in Figure 1, when heated under flowing air conditions, the lignin waste is steadily volatilized leading to a mass loss of ca. 41 wt % at 785 °C, after which, there is a sudden mass loss of a further 40 wt % due, presumably, to combustion of char. This leaves a noncombustible ash content of ca. 20 wt % as residue at 1000 °C (Figure 1). The TGA data indicates that the lignin waste contained a noncarbon mineral content of ca. 20 wt %, which ideally needed to be removed prior to the activation process. On the other hand, as shown in Figure 1, the LD hydrochar is completely burnt off at 550 °C, with most of the carbon combustion occurring between 420 and 550 °C. This indicates that the LD hydrochar is made up entirely of carbonaceous matter and therefore that the hydrothermal carbonization process dissolves any mineral waste to generate a carbon hydrochar. The LD hydrochar has a carbon content of 66.6%, and contains a high number of aromatic groups and aliphatic chains (see the Supporting Information, Appendix 1) as indicated by a high C/H ratio of 13.2. The hydrochar, being devoid of any mineral matter, was used as a carbon precursor for chemical activation with KOH.

Structural and Chemical Properties of Lignin-Derived Activated Carbons. The elemental composition of the LD hydrochar and activated carbons (Table 1) indicates that

Table 1. Elemental Composition (%) of Lignin-Derived LD Hydrochar, And the Yield, Composition and C/H Ratio of Lignin-Derived Activated Carbons

		elemental composition (%)			
sample	yield[a]	C	H	O	C/H ratio
LD hydrochar		66.6	5.06	28.34	13.2
LAC2600	35.6	67.8	1.36	30.84	49.9
LAC2700	27.0	83.3	0.50	16.20	166.6
LAC2800	20.8	85.9	0.35	13.75	254.4
LAC4600	20.2	75.3	1.33	23.37	56.6
LAC4700	18.7	78.3	0.52	21.18	150.6
LAC4800	14.5	84.9	0.41	14.69	207.1
LAC4900	8.7	92.6	0.36	7.04	257.2

[a]Measured in grams of activated carbon/100 grams of hydrochar.

activation of the hydrochar increases the carbon content from 66.6 wt % to between 68 and 93 wt % for the activated carbons; the remainder being mainly oxygen with a small amount of H. The H and O content of the activated carbons decreases at higher activation temperatures, with the effect that the C/H ratio rises to as high as ca. 260 for the most activated samples (LAC2800 and LAC4900). As expected, the activated carbon yield decreases at higher activation temperatures, and is higher for LAC2*T* samples compared to LAC4*T* analogues. The activated carbons do not possess any significant residual inorganic residues, as indicated by thermogravimetric analysis (see Figure S1 of the Supporting Information). Under heating in air, the activated carbon samples exhibit mass loss at two temperature regimes: below 100 °C and between 200 and 600 °C. The small (2−5 wt %) mass loss below 100 °C, due to evaporation of physisorbed water, is followed by greater mass loss between 200 and 580 °C due to the removal of volatile matter,[38] and combustion of the carbon framework (∼95 wt % of mass loss).[39] As activation temperature increases, the carbon burnoff temperature shifts to higher values and the burnoff temperature zone reduces indicating that the nature of carbon becomes more uniform, which is consistent with increase in the carbon content (Table 1). The rise in burnoff temperature for carbons activated at higher temperature suggests a probable increase in the level of graphitization. This is consistent with the powder XRD patterns (see Figure S2 of the Supporting Information), which show an apparent increase in the intensity of the peak at $2\theta = 43°$ for carbons activated at higher temperatures. This peak is ascribed to the (101) diffraction of graphitic carbon domains, whereas the (002) diffraction peak expected at $2\theta = 22$ is not clearly observed due to being masked by the gradient of the baseline. Overall, though, the (101) peaks are very broad, which suggests the presence of mainly amorphous carbon along with disordered turbostratic carbon.

The nitrogen sorption isotherms for activated carbons prepared at a KOH/carbon ratio of 2 are shown in Figure 2A. The isotherms of all three samples are type I, and typical for microporous materials. As activating temperature increases, there is a slight widening of the isotherm "knee", which may be attributed to presence of larger micropores. The changes in pore size are shown by the pore size distribution curves in Figure 2B and pore size given in Table 2. The carbons activated at a KOH/carbon ratio of 2 exhibit one main pore size maximum at 7 Å, along with a much smaller proportion of pores of size 9 and 12 Å. The pore size is remarkably similar for all three LAC2*T* samples, regardless of the activation temperature (600−800 °C). There is nevertheless a small but

DOI: 10.1021/acssuschemeng.5b00351
ACS Sustainable Chem. Eng. 2015, 3, 1658−1667

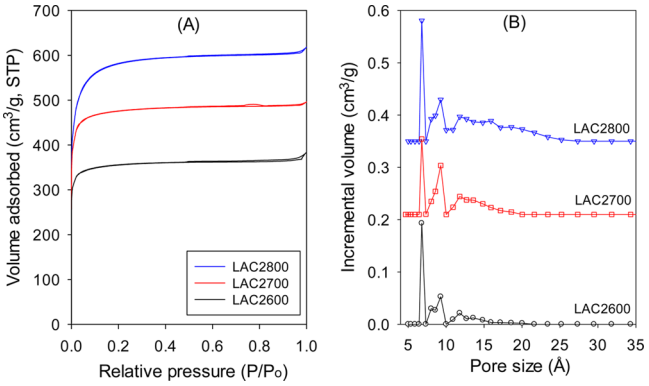

Figure 2. (A) Nitrogen sorption isotherms and (B) pore size distribution curves of lignin-derived carbon activated at 600−800 °C and KOH/carbon ratio of 2.

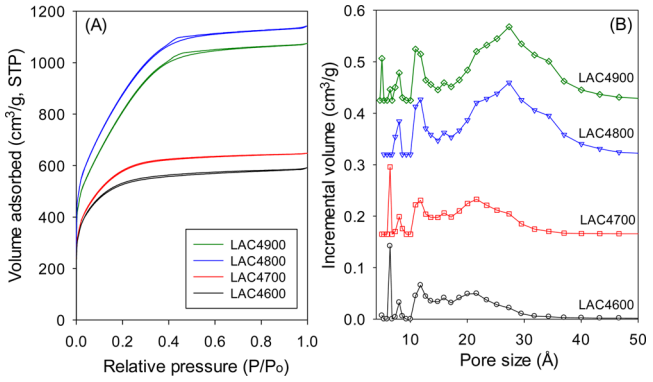

Figure 3. (A) Nitrogen sorption isotherms and (B) pore size distribution curves of lignin-derived carbon activated at 600−900 °C and KOH/carbon ratio of 4.

noticeable increase in the proportion of larger micropores (>10 Å) at higher activation temperatures. This increase in proportion of larger micropores may be ascribed to greater gasification caused by the CO_2 released by the decomposition of K_2CO_3 during the activation process.[10−13] As shown in Table 2, the LAC2*T* set of activated carbons has moderate to high surface area and pore volume; activation at 600 °C generates the lowest surface area and pore volume of 1159 m^2 g^{-1} and 0.59 cm^3 g^{-1}, respectively, whereas the highest values are after activation at 800 °C (1924 m^2 g^{-1} and 0.95 cm^3 g^{-1}). The proportion of microporosity for the LAC2*T* samples is very high; ≥97% of surface area and 93% of pore volume. This is among the highest levels of microporosity observed for activated carbons.[10−13] To put these values in context, we compared activation of lignin to cellulose.[28] Under similar conditions (700 °C and KOH/carbon = 2), lignin generates a carbon with higher porosity (surface area and pore volume) and microporosity than cellulose-derived carbon (designated as CAC2700 in Figure S3 and Table S1 of the Supporting Information). The lignin-derived sample has a much higher proportion of pores below 10 Å, which translates to a higher proportion (94%) of micropore volume compared to 84% for the cellulose-derived sample (see Table S1 of the Supporting Information). It is noteworthy that despite having high surface area, samples LAC2700 and LAC2800 are virtually entirely microporous. Our findings are consistent with previous reports that activation of lignin engenders the formation of micropores.[36]

The carbons activated at a KOH/carbon ratio of 4 exhibit higher porosity (compared to equivalent LCA2*T* samples) as shown by the nitrogen sorption isotherms in Figure 3A. The isotherms are typical for materials that possess micropores and small mesopores.[42] The higher amount of KOH leads to greater widening of the adsorption isotherm "knee" at low relative pressure compared to LAC2*T* equivalent samples. As shown in Figure 3B, the LAC4*T* samples exhibit relatively wide pore size distribution in the micropore/small mesopore size range with micropores centered at 6, 8 and 11 Å, and mesopores of size 20−27 Å. The greater amount of KOH in LAC4*T* samples increases the overall porosity and pore size via gasification especially at 700 °C and above.[10−13,43] The least activated LAC4*T* sample (LAC4600) has a surface area and pore volume of 1820 m^2 g^{-1} and 0.91 cm^3 g^{-1}, respectively (Table 3). The porosity rises at higher activation temperature to a maximum at 800 °C and then decreases at 900 °C. We note that surface area and pore volume of 3235 m^2 g^{-1} and 1.77 cm^3 g^{-1}, respectively, achieved at 800 °C are the highest reported so far for lignin-derived activated carbons.[36]

Comparison of activation of lignin to that of cellulose at KOH/carbon ratio of 4 revealed some interesting trends. For activation at 600 and 700 °C, the activated carbons derived from both precursors have comparable surface area and pore volume (see Figure S4 and Table S1 of the Supporting Information). The proportion of micropore surface area (ca. 90%) and micropore volume (ca. 85%) is also similar (see Table S1 of the Supporting Information). However, when the activation temperature is increased to 800 °C, a clear distinction is observed; although the surface area of the lignin-derived sample (LAC4800) increases further from 2038 m^2 g^{-1} at 700 °C to 3235 m^2 g^{-1} at 800 °C, that of the cellulose-derived sample decreases from 2370 to 2047 m^2 g^{-1}. This means that, as discussed above, the maximum surface area for LAC4*T* samples is achieved at 800 °C, whereas for

Table 2. Textural Properties and Gas (CO_2 and Hydrogen) Uptake of Lignin-Derived Activated Carbons Prepared at KOH/Carbon Ratio of 2

				CO_2 uptake[d] (mmol g^{-1})				
				25 °C		0 °C		
sample	surface area[a] (m^2 g^{-1})	pore volume[b] (cm^3 g^{-1})	pore size[c] (Å)	1 bar	20 bar	1 bar	20 bar	H_2 uptake[e] (wt %)
LAC2600	1157 (1123)	0.59 (0.54)	7/9/12	3.2	7.3	4.4	7.7	3.2 (3.6)
LAC2700	1551 (1502)	0.77 (0.72)	7/9/12	4.6	15.1	7.4	16.8	3.7 (4.4)
LAC2800	1924 (1839)	0.95 (0.87)	7/9/13	4.0	17.3	6.5	20.1	4.7 (5.6)

[a]The values in the parentheses are micropore surface area. [b]The values in the parentheses are micropore volume. [c]Pore size distribution maxima from NLDFT analysis. [d]CO_2 uptake at 0 and 25 °C and 1 or 20 bar. [e]Excess H_2 uptake at −196 °C and 20 bar; values in parentheses are total H_2 uptake.

DOI: 10.1021/acssuschemeng.5b00351
ACS Sustainable Chem. Eng. 2015, 3, 1658−1667

Table 3. Textural Properties and Gas (CO_2 and Hydrogen) Uptake of Lignin-Derived Activated Carbons Prepared at KOH/Carbon Ratio of 4

sample	surface area[a] ($m^2\ g^{-1}$)	pore volume[b] ($cm^3\ g^{-1}$)	pore size[c] (Å)	CO_2 uptake[d] (mmol g^{-1})	H_2 uptake[e] (wt %)
LAC4600	1820 (1627)	0.91 (0.75)	6/8/11/20	2.7	3.5 (4.2)
LAC4700	2038 (1832)	1.00 (0.84)	6/8/11/21	3.2	4.4 (5.2)
LAC4800	3235 (1978)	1.77 (0.93)	8/11/27	2.8	4.8 (6.0)
LAC4900	2750 (792)	1.66 (0.43)	5/8/11/27	2.4	5.2 (6.2)

[a]The values in the parentheses are micropore surface area. [b]The values in the parentheses are micropore volume. [c]Pore size distribution maxima from NLDFT analysis. [d]CO_2 uptake at 25 °C and 1 bar. [e]Excess H_2 uptake at −196 °C and 20 bar; the values in parentheses are total H_2 uptake.

equivalent cellulose-derived samples the maximum surface area is achieved at a lower temperature of 700 °C (see Figure S5 of the Supporting Information). Both the total and micropore surface area for cellulose-derived carbons show a maxima at 700 °C, whereas lignin-derived samples show an increase up to 800 °C (see Figure S5 of the Supporting Information). These findings indicate that lignin is indeed harder to activate than cellulose, and that it can sustain harsher activation conditions while still retaining high surface area in a manner that is not observed for cellulose.[36]

CO_2 Uptake. It is widely accepted that the presence of micropores is a main factor for CO_2 uptake in porous materials. Prompted by the high microporosity and relatively narrow pore size distribution of the LAC2*T* set of samples, we explored their CO_2 uptake. The CO_2 uptake isotherms for the LAC2*T* set of samples at ambient temperature (25 °C) are shown in Figure 4A, and the amount of CO_2 stored at 1 and 20 bar is given in

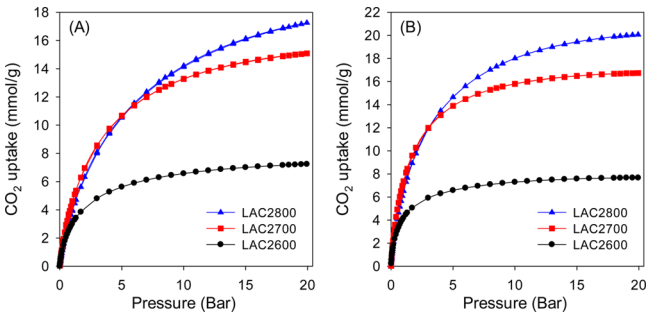

Figure 4. CO_2 uptake isotherms at (A) 25 °C and (B) 0 °C in the pressure range 0−20 bar for lignin-derived LAC2*T* carbons.

Table 2. At 25 °C, sample LAC2700 shows the highest uptake at low pressure (<5 bar), whereas sample LAC2800 stores more CO_2 at 20 bar. Thus, under ambient conditions (25 °C and 1 bar; see Figure S6 of the Supporting Information), sample LAC2600 has CO_2 uptake of 3.2 mmol g^{-1}, whereas for sample LAC2700 and LAC2800 it is 4.6 and 4.0 mmol g^{-1}, respectively. Given the relatively similar pore size distribution for samples LAC2600 and LAC2700 (Figure 2), the greater CO_2 uptake of the latter is attributable to higher surface area. The trend of increase in uptake at higher surface area is, however, not evident for sample LAC2800 due to a slight broadening of pore size (i.e., presence of a significant proportion of pores of size >15 Å). These observations indicate that the pore size and particularly the presence of micropores of size ca. 7 Å is the key factor in determining the CO_2 uptake under ambient conditions. The observed dependence of CO_2 uptake at ambient conditions on pore size is consistent with previous reports.[21−27] As shown in Figure 4A, the CO_2 uptake at 20 bar is more dependent on the total surface area with samples LAC2700 and LAC2800 exhibiting much higher storage capacity of up to 17.3 mmol g^{-1}. The observed CO_2 uptake of up to 4.6 mmol g^{-1}, at 25 °C and 1 bar is among the highest observed for all kinds of porous carbons and is in the top performance range of materials that include the very best activated carbons,[21−26,44−50] and templated carbons.[27,51−54]

Figure 4B shows the CO_2 uptake isotherms for LAC2*T* carbons at 0 °C. At 1 bar, the uptake is in the range 4.4 and 7.4 mmol g^{-1} (Table 1, and Figure S7 of the Supporting Information). The CO_2 uptake of 7.4 mmol g^{-1} exhibited by sample LAC2700 at 1 bar and 0 °C is one of the highest so far reported for porous materials.[44−54] At low pressure (<3 bar), sample LAC2700 has the higher uptake whereas at pressures above ca. 3.5 bar, the uptake of sample LAC2800 is greater reaching a high of 20.1 mmol g^{-1} at 20 bar. The uptake at 0 °C is thus more significantly dependent on the total surface area. As shown in Table 3 the CO_2 uptake of the LAC4*T* set of samples is lower than that of the LAC2*T* set and varies between 2.4 and 3.2 mmol g^{-1} at 25 °C and 1 bar. LAC4*T* samples have much wider pore size distribution which includes a large proportion of mesopores that are poor stores for CO_2. This is consistent with theoretical calculations that suggest enhancement of the adsorption potential for slit-shaped pore channels that are twice the diameter of adsorbing molecule.[55,56] Pores of ca. 7 Å are ideal for CO_2 (diameter of ca. 3.3 Å).

The importance of 7 Å pores in CO_2 uptake is highlighted by a comparison of the room temperature storage capacity of sample LAC2700 with that of the equivalent cellulose-derived sample (see Figure S8 of the Supporting Information). At 1 bar, the cellulose-derived sample (CAC2700) has CO_2 uptake of 2.8 mmol g^{-1}, which is significantly lower than that (4.6 mmol g^{-1}) of the equivalent lignin-derived sample. Given that CO_2 uptake at 25 °C and 1 bar does not strongly relate to the surface area, we ascribe the higher uptake of the lignin-derived sample to the presence of a significant proportion of 7 Å pores (see Figure S3 of the Supporting Information). Although both samples, LAC2700 and CAC2700, are highly microporous (see Table S1 of the Supporting Information), the latter has hardly any "optimum" micropores of size <8 Å. This observation is consistent with previous reports on the importance of small micropores in CO_2 uptake,[45,47] and indicates that hydrothermally carbonized lignin is a good source for activated carbons for CO_2 storage applications. As expected, at a pressure of 20 bar, the LAC2700 sample has higher CO_2 uptake of 15.1 mmol g^{-1} compared to 12.5 mmol g^{-1} for CAC2700 (see Figure S8 of the Supporting Information), due to higher surface area of the former.

The high efficiency of CO_2 uptake in samples LAC2600 and LAC2700 should be accompanied by enhanced CO_2-carbon surface interaction. A measure of such interaction, the isosteric heat of adsorption (Q_{st}), was calculated by applying the Clausius−Clapeyron equation to the CO_2 adsorption isotherms at 0 and 25 °C and is shown in Figure 5 as a function of CO_2

DOI: 10.1021/acssuschemeng.5b00351
ACS Sustainable Chem. Eng. 2015, 3, 1658−1667

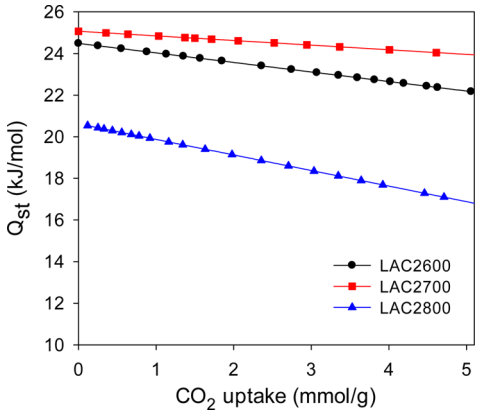

Figure 5. Isosteric heat of CO_2 adsorption (Q_{st}) as a function of CO_2 uptake for LAC2*T* samples.

uptake. The Q_{st} at near zero CO_2 coverage for LAC2600 (24.5 kJ mol^{-1}) and LAC2700 (25.1 kJ mol^{-1}) is higher than that of LAC2800 (20.5 kJ mol^{-1}). In general, the Q_{st} for the LAC2*T* samples is in the range of what is typically observed for porous carbons.[44−54] It is interesting to note that the CO_2 uptake densities (at 25 °C and 1 bar) for LAC2600 (2.8 μmol m^{-2}) and LAC2700 (3.0 μmol m^{-2}) are comparable and significantly higher than for LAC2800 (2.1 μmol m^{-2}). The CO_2 uptake density of the LAC4*T* set of samples is much lower at ca. 1.5 μmol m^{-2} for LAC4600 and LAC4700 and ca. 0.9 μmol m^{-2} for LAC4800 and LAC4900. The CO_2 uptake density clearly reduces as the proportion and size of mesopores rises (Tables 2 and 3). It appears therefore that the presence of larger pores (i.e., >7 Å) is detrimental to CO_2 uptake even in cases where there are still a significant proportion of the optimal 7 Å pores as typified by the behavior of sample LAC2800.

For postcombustion CO_2 capture, commercial viability considerations require that usable materials capture at least 2 mmol g^{-1} at 50 °C and above.[57,58] We explored the uptake of the LAC2*T* carbons at 50 and 75 °C (Figure 6, and Figure S9 of the Supporting Information). All three LAC2*T* samples show attractive CO_2 uptake at 50 °C; LAC2600 stores 2.0 and 4.4 mmol g^{-1} at 1 and 10 bar, respectively, and the corresponding uptake for LAC2700 is higher at 2.5 and 6.8 mmol g^{-1} whereas for LAC2800 it is 2.3 and 6.9 mmol g^{-1}. The carbons reach the threshold for commercial viability in CO_2 capture from postcombustion flue gases.[57,58] At 75 °C, the samples still retain attractive CO_2 uptake (at 1 and 5 bar respectively) of 1.3−1.6 and 3.3−4.8 mmol g^{-1}. We attribute the relatively high uptake for sample LAC2700 to higher Q_{st} values as discussed above. Higher Q_{st} values also explains the observation that at a pressure of 0.15 bar, samples LAC2700 and LAC2600 have higher CO_2 uptake (ca. 0.6 and 0.35 mmol g^{-1} at 50 and 75 °C, respectively) compared to 0.5 and 0.28 mmol g^{-1} for LAC2800. At 75 °C and 7.4 bar;[59] both samples LAC2700 and LAC2800 have uptakes of 6.1 mmol g^{-1}, which is higher than that of benchmark materials; hierarchical carbons (5.7 mmol g^{-1}) and polyethylenimine impregnated graphene−silica sheets (4.3 mmol g^{-1}).[60]

Hydrogen Uptake. The hydrogen uptake isotherms for the lignin-derived carbons are shown in Figure 7, and the excess and total uptake at 20 bar is summarized in Tables 2 and 3. Our measurements determine the excess hydrogen uptake, from which the total amount stored is calculated using established procedures (see Appendix 2 of the Supporting Information).[61,62] Except for LAC2600 and LAC2700, the samples do not reach (or approach) saturation, which suggests that higher uptake is possible at pressures above 20 bar. For LAC2*T* samples, the hydrogen uptake rises with surface area; at 20 bar, LAC2600 stores 3.2 wt % compared to 3.7 and 4.7 wt % for LAC2700 and LAC2800, respectively, with corresponding total uptake in the range 3.6 to 5.6 wt %. The hydrogen uptake of the LAC4*T* samples increases at higher activation temperatures; the excess uptake increases from 3.5 to 5.2 wt %, whereas the total uptake is in the range 4.2 to 6.2 wt %. Overall, the hydrogen uptake of the lignin-derived carbons is comparable to that of the best activated carbons and templated carbons of similar surface area.[10−12,29,32,61,63−78]

The total hydrogen uptake of both sets of carbons is plotted as a function of total surface area in Figure 8. The plot is useful in showing the trend in hydrogen uptake density, which is, in turn, a measure of the efficiency of the pore channels of each sample in storing hydrogen. From Figure 8, it is apparent that the hydrogen uptake of LAC2*T* samples increases linearly with surface area. This is unsurprising given that this set of samples shows very similar pore size distribution. We have previously

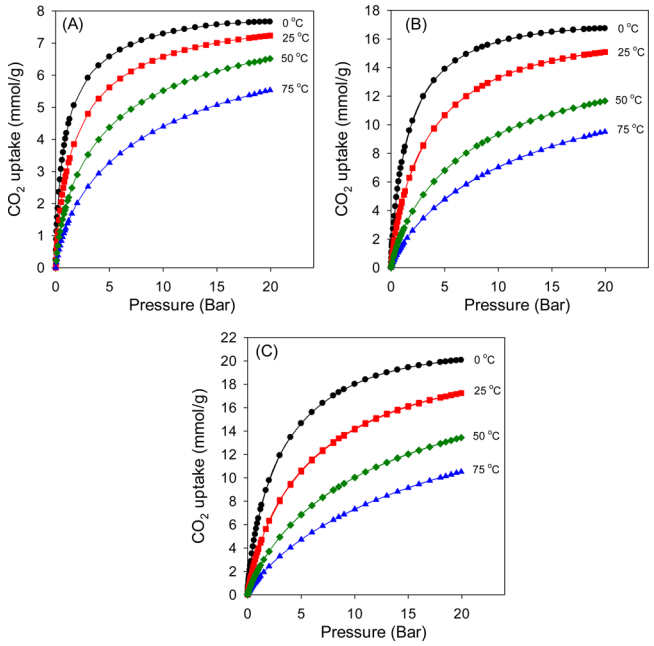

Figure 6. CO_2 uptake isotherms for samples (A) LAC2600, (B) LAC2700 and (C) LAC2800 at various temperatures.

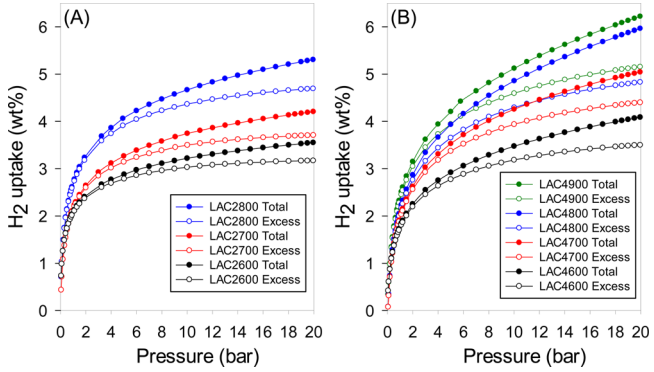

Figure 7. Hydrogen uptake of lignin-derived samples: (A) LAC2*T* and (B) LAC4*T*.

DOI: 10.1021/acssuschemeng.5b00351
ACS Sustainable Chem. Eng. 2015, 3, 1658−1667

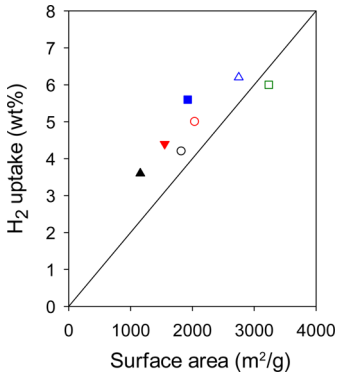

Figure 8. Hydrogen uptake as a function of surface area for LAC2*T* (filled symbols) and LAC4*T* (open symbols) carbons. The solid line represents the Chahine rule.

shown that for samples with similar pore size distribution, the surface area is a good predictor of trends in hydrogen uptake within any given group of such materials.[79] Thus, a linear relationship (slope = 2.9 × 10^{-3} wt %/(m^2 g^{-1}), which is equivalent to a hydrogen uptake density of 14.5 μmol H_2 m^{-2}, is observed for LAC2*T* samples. The LAC2*T* carbons outperform the Chahine rule (slope = 10 μmol H_2 m^{-2}),[80] depicted by the solid line in Figure 8. For LAC4*T* samples, a linear relationship is less clear and the slope is 2.24 × 10^{-3} wt %/(m^2 g^{-1}), equivalent to a hydrogen uptake density of 11.2 μmol H_2 m^{-2}, which is closer to that predicted by the Chahine rule and comparable to KOH activated carbide-derived carbons (11.8 ± 0.7 μmol H_2 m^{-2})[64] and KOH activated zeolite-templated carbons (10.7 ± 0.8 μmol H_2 m^{-2}).[65] The hydrogen storage density of the lignin-derived carbons, and in particular the LAC2*T* set of samples, is superior to what has previously been reported for several classes of carbons, including (i) CO_2 activated carbide-derived carbons (9 ± 0.1 μmol H_2 m^{-2}),[81] (ii) carbon nanostructures consisting of activated carbons and CNTs (9.55 μmol H_2 m^{-2})[75] and activated carbons, SWNTs, SWNHs, GCFs (11.75 μmol H_2 m^{-2}) (−196 °C and 20 bar)[82] and (iii) chemically activated carbons obtained from anthracite (9 ± 0.1 μmol H_2 m^{-2}).[61]

When compared to equivalent cellulose-derived carbons, the hydrogen uptake of the ligin-derived samples is generally higher (see Figure S10 of the Supporting Information). For example, the hydrogen uptake of sample LAC2700 is higher than that of equivalent cellulose-derived sample CAC2700 (see Figure S10A of the Supporting Information); at 20 bar, the uptake is 4.4 wt % for LAC2700 and 3.6 wt % for CAC2700. Furthermore, the fact that the lignin-derived samples can withstand harsher activation conditions while still generating higher surface area carbons means that the maximum achievable hydrogen uptake is also greater for the lignin-derived activated carbons (see Figure S10B of the Supporting Information). Thus, the uptake of the lignin-derived samples can reach 6.2 wt % compared to a high of 5.6 wt % for cellulose-derived carbons (see Table S1 of the Supporting Information).

CONCLUSIONS

In summary, chemical activation of cheap, renewable and readily available hydrothermally carbonized lignin-derived hydrochar with KOH has been demonstrated as a route to highly microporous carbons with excellent gas sorption properties. The hydrothermal carbonization converts lignin waste into a fully carbonaceous and activateable hydrochar product. Activated carbons prepared at KOH/carbon ratios of 2 (LAC2*T* set) and 4 (LAC4*T* set) exhibit moderate to high surface area and pore volume in the range 1157−1924 m^2 g^{-1} and 0.59−0.95 cm^3 g^{-1} for the former and 1820−3235 m^2 g^{-1} and 0.91−1.77 cm^3 g^{-1} for the latter. The lignin-derived hydrochar is harder to activate than cellulose-derived hydrochar and thus can sustain harsher activation conditions while still retaining high surface area. The carbons prepared at a KOH/carbon ratio of 2 (LAC2*T* samples) are highly microporous and dominated by pores of size 7 Å, and therefore exhibit enhanced CO_2 uptake of 3.2−4.6 mmol g^{-1} at 25 °C and ambient pressure, whereas CO_2 uptake of LAC4*T* samples is in the range 2.4−3.2 mmol g^{-1}. Under similar activation conditions, the lignin-derived carbons possess 7 Å pores compared to equivalent cellulose-derived carbons that have larger (>8 Å) micropores, which translates to better CO_2 uptake for the former. The best CO_2 absorber at ambient temperature (sample LAC2700) also shows attractive uptake at 50 and 75 °C, and high isosteric heat of CO_2 adsorption (Q_{st}) of 25 kJ mol^{-1}. For hydrogen storage, the total uptake (at −196 °C and 20 bar) is 3.6−5.6 wt % for LAC2*T* samples, and is higher (4.2−6.2 wt %) for LAC4*T* samples. The LAC2*T* samples exhibit one of the highest hydrogen uptake densities ever reported (14.5 μmol H_2 m^{-2}), which is at least 50% higher than those for most porous carbons.

ASSOCIATED CONTENT

Supporting Information

Two appendices, one table and 10 figures describing nature of lignin used, calculation of total hydrogen stored, thermogravimetric and porosity data and gas uptake data. The Supporting Information is available free of charge on the ACS Publications website at DOI: 10.1021/acssuschemeng.5b00351.

AUTHOR INFORMATION

Corresponding Author

*R. Mokaya. E-mail: r.mokaya@nottingham.ac.uk.

Notes

The authors declare no competing financial interest.

ACKNOWLEDGMENTS

We thank the Rajamangala University of Technology Srivijaya (RMUTSV), Thailand for funding and a studentship for W.S. We thank Borregaard LignoTech for the lignin.

REFERENCES

(1) Morris, R. E.; Wheatley, P. S. Gas storage in nanoporous materials. *Angew. Chem., Int. Ed.* **2008**, *47*, 4966−4981.
(2) van den Berg, A. W. C.; Arean, C. O. Materials for hydrogen storage: Current research trends and perspectives. *Chem. Commun.* **2008**, 668−681.
(3) Schlapbach, L.; Zuttel, A. Hydrogen-storage materials for mobile applications. *Nature* **2001**, *414*, 353−358.
(4) Turner, J. A. A realizable renewable energy future. *Science* **1999**, *285*, 687−689.
(5) Crabtree, G. W.; Dresselhaus, M. S.; Buchanan, M. V. The hydrogen economy. *Phys. Today* **2004**, *57*, 39−44.
(6) Winter, C.-J. Hydrogen energy - Abundant, efficient, clean: A debate over the energy-system-of-change. *Int. J. Hydrogen Energy* **2009**, *34*, 1−52.
(7) Ma, X.; Wang, X.; Song, C. "Molecular basket" sorbents for separation of CO_2 and H_2S from various gas streams. *J. Am. Chem. Soc.* **2009**, *131*, 5777−5783.

DOI: 10.1021/acssuschemeng.5b00351
ACS Sustainable Chem. Eng. 2015, 3, 1658−1667

(8) Wang, Q.; Luo, J.; Zhong, Z.; Borgna, A. CO_2 capture by solid adsorbents and their applications: Current status and new trends. *Energy Environ. Sci.* **2011**, *4*, 42−55.
(9) Zhang, L. L.; Zhao, X. S. Carbon-based materials as supercapacitor electrodes. *Chem. Soc. Rev.* **2009**, *38*, 2520−2531.
(10) Xia, Y. X.; Yang, Z. X.; Zhu, Y. Porous carbon-based materials for hydrogen storage: Advancement and challenges. *J. Mater. Chem. A* **2013**, *1*, 9365−9381.
(11) Wang, J. C.; Kaskel, S. KOH activation of carbon-based materials for energy storage. *J. Mater. Chem.* **2012**, *22*, 23710−23725.
(12) Sevilla, M.; Mokaya, R. Energy storage applications of activated carbons: Supercapacitors and hydrogen storage. *Energy Environ. Sci.* **2014**, *7*, 1250−1280.
(13) Wei, L.; Yushin, G. Nanostructured activated carbons from natural precursors for electrical double layer capacitors. *Nano Energy* **2012**, *1*, 552−565.
(14) Choi, S.; Drese, J. H.; Jones, C. W. Adsorbent materials for carbon dioxide capture from large anthropogenic point sources. *ChemSusChem* **2009**, *2*, 796−854.
(15) Adeniran, B.; Mokaya, R. Low temperature synthesized carbon nanotube superstructures with superior CO_2 and hydrogen storage capacity. *J. Mater. Chem. A* **2015**, *3*, 5148−5161.
(16) D'Alessandro, D. M.; Smit, B.; Long, J. R. Carbon dioxide capture: Prospects for new materials. *Angew. Chem., Int. Ed.* **2010**, *49*, 6058−6082.
(17) Wang, S.; Yan, S.; Ma, X.; Gong, J. Recent advances in capture of using alkali-metal-based oxides. *Energy Environ. Sci.* **2011**, *4*, 3805−3819.
(18) Sumida, K.; Rogow, D. L.; Mason, J. A.; McDonald, T. M.; Bloch, E. D.; Herm, Z. R.; Bae, T.-H.; Long, J. R. Carbon dioxide capture in metal-organic frameworks. *Chem. Rev.* **2012**, *112*, 724−781.
(19) Furukawa, H.; Ko, N.; Go, Y. B.; Aratani, N.; Choi, S. B.; Choi, E.; Yazaydin, A. O.; Snurr, R. Q.; O'Keeffe, M.; Kim, J.; Yaghi, O. M. Ultra-high porosity in metal−organic frameworks. *Science* **2010**, *329*, 424−428.
(20) Yazaydin, A. O.; Benin, A. I.; Faheem, S. A.; Jakubczak, P.; Low, J. J.; Willis, R. R.; Snurr, R. Q. Enhanced CO_2 adsorption in metal-organic frameworks via occupation of open-metal sites by coordinated water molecules. *Chem. Mater.* **2009**, *21*, 1425−1430.
(21) (a) Sevilla, M.; Fuertes, A. B. Sustainable porous carbons with a superior performance for CO2 capture. *Energy Environ. Sci.* **2011**, *4*, 1765−1771. (b) Sevilla, M.; Valle-Vigon, P.; Fuertes, A. B. N-Doped polypyrrole-based porous carbons for CO_2 capture. *Adv. Funct. Mater.* **2011**, *21*, 2781−2787.
(22) Presser, V.; McDonough, J.; Yeon, S.-H.; Gogotsi, Y. Effect of pore size on carbon dioxide sorption by carbide derived carbon. *Energy Environ. Sci.* **2011**, *4*, 3059−3066.
(23) Nandi, M.; Okada, K.; Dutta, A.; Bhaumik, A.; Maruyama, J.; Derksa, D.; Uyama, H. Unprecedented CO_2 uptake over highly porous N-doped activated carbon monoliths prepared by physical activation. *Chem. Commun.* **2012**, *48*, 10283−10285.
(24) Silvestre-Albero, J.; Wahby, A.; Sepulveda-Escribano, A.; Martinez-Escandell, M.; Kaneko, K.; Rodriguez-Reinoso, F. Ultrahigh CO_2 adsorption capacity on carbon molecular sieves at room temperature. *Chem. Commun.* **2011**, *47*, 6840−6842.
(25) Masika, E.; Mokaya, R. High surface area metal salt templated carbon aerogels via a simple subcritical drying route: Preparation and CO_2 uptake properties. *RSC Adv.* **2013**, *3*, 17677−17681.
(26) Yang, Z.; Xia, Y.; Zhu, Y. Preparation of sulfur-doped microporous carbons for the storage of hydrogen and carbon dioxide. *Carbon* **2012**, *50*, 5543−5553.
(27) Xia, Y. D.; Mokaya, R.; Walker, G. S.; Zhu, Y. Q. Superior CO_2 adsorption capacity on N-doped, high-surface-area, microporous carbons templated from zeolite. *Adv. Energy Mater.* **2011**, *1*, 678−683.
(28) Sevilla, M.; Fuertes, A. B.; Mokaya, R. High density hydrogen storage in superactivated carbons from hydrothermally carbonized renewable organic materials. *Energy Environ. Sci.* **2011**, *3*, 1400−1410.
(29) (a) Yang, Z.; Xia, Y.; Mokaya, R. Enhanced hydrogen storage capacity of high surface area zeolite-like carbon materials. *J. Am. Chem. Soc.* **2007**, *129*, 1673−1679. (b) Masika, E.; Mokaya, R. Exceptional gravimetric and volumetric hydrogen storage for densified zeolite templated carbons with high mechanical stability. *Energy Environ. Sci.* **2014**, *7*, 427−434.
(30) Montoya, A.; Mondragon, F.; Truong, T. N. CO_2 adsorption on carbonaceous surfaces: A combined experimental and theoretical study. *Carbon* **2003**, *41*, 29−39.
(31) Sevilla, M.; Mokaya, R.; Fuertes, A. B. Ultrahigh surface area polypyrrole-based carbons with superior performance for hydrogen storage. *Energy Environ. Sci.* **2011**, *4*, 2930−2936.
(32) (a) Hu, B.; Wang, K.; Wu, L.; Yu, S. H.; Antonietti, M.; Titirici, M. M. Engineering carbon materials from the hydrothermal carbonization process of biomass. *Adv. Mater.* **2010**, *22*, 813−828. (b) Titirici, M. M.; Antonietti, M. Chemistry and materials options of sustainable carbon materials made by hydrothermal carbonization. *Chem. Soc. Rev.* **2010**, *39*, 103−116. (c) Titirici, M. M.; White, R. J.; Falco, C.; Sevilla, M. Black perspectives for a green future: Hydrothermal carbons for environment protection and energy storage. *Energy Environ. Sci.* **2012**, *5*, 6796−6822.
(33) Kang, S.; Li, X.; Fan, J.; Chang, J. Characterization of hydrochars produced by hydrothermal carbonization of lignin, cellulose, D-xylose, and wood meal. *Ind. Eng. Chem. Res.* **2012**, *51*, 9023−9031.
(34) Libra, J. A.; Ro, K. S.; Kammann, C.; Funke, A.; Berge, N. D.; Neubauer, Y.; Titirici, M.-M.; Fuhner, C.; Bens, O.; Kern, J.; Emmerich, K.-H. Hydrothermal carbonization of biomass residuals: A comparative review of the chemistry, processes and applications of wet and dry pyrolysis. *Biofuels* **2011**, *2*, 71−106.
(35) Tuck, C. O.; Pérez, E.; Horváth, I. T.; Sheldon, R. A.; Poliakoff, M. Valorization of biomass: Deriving more value from waste. *Science* **2012**, *337*, 695−699.
(36) (a) Suhas; Carrott, P. J. M.; Ribeiro Carrott, M. M. L. Lignin − From natural adsorbent to activated carbon: A review. *Bioresour. Technol.* **2007**, *98*, 2301−2312. (b) Hayashi, J.; Kazehaya, A.; Muroyama, K.; Watkinson, A. P. Preparation of activated carbon from lignin by chemical activation. *Carbon* **2000**, *38*, 1873−1878. (c) Gonzalez-Serrano, E.; Cordero, T.; Rodriguez-Mirasol, J.; Cotoruelo, L.; Rodriguez, J. J. Removal of water pollutants with activated carbons prepared from H_3PO_4 activation of lignin from kraft black liquors. *Water Res.* **2004**, *38*, 3043−3050. (d) Fierro, V.; Torne-Fernandez, V.; Celzard, A.; Montane, D. Influence of the demineralisation on the chemical activation of Kraft lignin with orthophosphoric acid. *J. Hazard. Mater.* **2007**, *149*, 126−133. (e) Fierro, V.; Torne-Fernandez, V.; Celzard, A. Methodical study of the chemical activation of Kraft lignin with KOH and NaOH. *Microporous Mesoporous Mater.* **2007**, *101*, 419−431.
(37) (a) Daud, W. M. A. W.; Ali, W. S. W. Comparison on pore development of activated carbon produced from palm shell and coconut shell. *Bioresour. Technol.* **2004**, *93*, 63−69. (b) Sharma, R. K.; Wooten, J. B.; Baliga, V. L.; Lin, X.; Chan, W. G.; Hajaligol, M. R. Characterization of chars from pyrolysis of lignin. *Fuel* **2004**, *83*, 1469−1482.
(38) Fang, Z.; Sato, T.; Smith, R. L., Jr.; Inomata, H.; Arai, K.; Kozinski, J. A. Reaction chemistry and phase behavior of lignin in high-temperature and supercritical water. *Bioresour. Technol.* **2008**, *99*, 3424−3430.
(39) (a) Jakab, E.; Faix, O.; Till, F. Thermal decomposition of milled wood lignins studied by thermogravimetry/mass spectrometry. *J. Anal. Appl. Pyrolysis* **1997**, *40*−*41*, 171−186. (b) Tejado, A.; Pena, C.; Labidi, J.; Echeverria, J. M.; Mondragon, I. Physico-chemical characterization of lignins from different sources for use in phenol−formaldehyde resin synthesis. *Bioresour. Technol.* **2007**, *98*, 1655−1663.
(40) (a) Jin, W.; Singh, K.; Zondlo, J. Pyrolysis kinetics of physical components of wood and wood-polymers using isoconversion wethod. *Agriculture* **2013**, *3*, 12−32. (b) Yang, H.; Yan, R.; Chen, H.; Zheng, C.; Lee, D. H.; Liang, D. T. In-depth investigation of biomass pyrolysis based on three major components: Hemicellulose, cellulose and lignin. *Energy Fuels* **2006**, *20*, 388−393. (c) Brebu, M.; Vasile, C. Thermal

DOI: 10.1021/acssuschemeng.5b00351
ACS Sustainable Chem. Eng. 2015, 3, 1658−1667

degradation of lignin - A review. *Cellu. Chem. Technol.* **2010**, *44*, 353−363.
(41) Liu, L.; Deng, Q.-F.; Hou, X.-X.; Yuan, Z.-Y. User-friendly synthesis of nitrogen-containing polymer and microporous carbon spheres for efficient CO_2 capture. *J. Mater. Chem.* **2012**, *22*, 15540−15548.
(42) (a) Sing, K. S. W. The use of gas adsorption for the characterization of porous solids. *Colloids Surf.* **1989**, *38*, 113−124. (b) Kruk, M.; Jaroniec, M.; Gadkaree, K. P. Determination of the specific surface area and the pore size of microporous carbons from adsorption potential distributions. *Langmuir* **1999**, *15*, 1442−1448.
(43) Díaz-Terán, J.; Nevskaia, D. M.; Fierro, J. L. G.; López-Peinado, A. J.; Jerez, A. Study of chemical activation process of a lignocellulosic material with KOH by XPS and XRD. *Microporous Mesoporous Mater.* **2003**, *60*, 173−181.
(44) Wahby, A.; Ramos-Fernandez, J. M.; Martnez-Escandell, M.; Sepulveda-Escribano, A.; Silvestre-Albero, J.; Rodriguez-Reinoso, F. High-surface-area carbon molecular sieves for selective CO_2 adsorption. *ChemSusChem* **2010**, *3*, 974−981.
(45) Sevilla, M.; Parra, J. B.; Fuertes, A. B. Assessment of the role of micropore size and N-doping in CO_2 capture by porous carbons. *ACS Appl. Mater. Interfaces* **2013**, *5*, 6360−6368.
(46) (a) Wickramaratne, N. P.; Jaroniec, M. Importance of small micropores in CO_2 capture by phenolic resin-based activated carbon spheres. *J. Mater. Chem. A* **2013**, *1*, 112−116. (b) Wickramaratne, N. P.; Jaroniec, M. Activated carbon spheres for CO_2 adsorption. *ACS Appl. Mater. Interfaces* **2013**, *5*, 1849−1855.
(47) Zhang, Z.; Zhou, J.; Xing, W.; Xue, Q.; Yan, Z.; Zhuo, S.; Qiao, S. Z. Critical role of small micropores in high CO_2 uptake. *Phys. Chem. Chem. Phys.* **2013**, *15*, 2523−2529.
(48) Fan, X.; Zhang, L.; Zhang, G.; Shu, Z.; Shi, J. Chitosan derived nitrogen-doped microporous carbons for high performance CO_2 capture. *Carbon* **2013**, *61*, 423−430.
(49) Zhao, Y.; Zhao, L.; Yao, K. X.; Yang, Y.; Zhang, Q.; Han, Y. Novel porous carbon materials with ultrahigh nitrogen contents for selective CO_2 capture. *J. Mater. Chem.* **2012**, *22*, 19726−19731.
(50) Lee, D.; Zhang, C.; Wei, C.; Ashfeld, B. L.; Gao, H. Hierarchically porous materials via assembly of nitrogen-rich polymer nanoparticles for efficient and selective CO_2 capture. *J. Mater. Chem. A* **2013**, *1*, 14862−14867.
(51) Robertson, C.; Mokaya, R. Microporous activated carbon aerogels via a simple subcritical drying route for CO_2 capture and hydrogen storage. *Microporous Mesoporous Mater.* **2013**, *179*, 151−156.
(52) Almasoudi, A.; Mokaya, R. Porosity modulation of activated ZIF-templated carbons via compaction for hydrogen and CO_2 storage applications. *J. Mater. Chem. A* **2014**, *2*, 10960−10968.
(53) Almasoudi, A.; Mokaya, R. A CVD route for the preparation of templated and activated carbons for gas storage applications using zeolitic imidazolate frameworks (ZIFs) as template. *Microporous Mesoporous Mater.* **2014**, *195*, 258−265.
(54) Adeniran, B.; Masika, E.; Mokaya, R. A family of microporous carbons prepared via a simple metal salt carbonization route with high selectivity for exceptional gravimetric and volumetric post-combustion CO_2 capture. *J. Mater. Chem. A* **2014**, *2*, 14696−14710.
(55) Wei, H.; Deng, S.; Hu, B.; Chen, Z.; Wang, B.; Huang, J.; Yu, G. Granular bamboo-derived activated carbon for high CO_2 adsorption: The dominant role of narrow micropores. *ChemSusChem* **2012**, *5*, 2354−2360.
(56) Everett, D. H.; Powl, J. C. Adsorption in slit-like and cylindrical micropores in the henry's law region. A model for the microporosity of carbons. *J. Chem. Soc., Faraday Trans. 1* **1976**, *72*, 619−636.
(57) Gray, M. L.; Champagne, K. J.; Fauth, D.; Baltrus, J. P.; Pennline, H. Performance of immobilized tertiary amine solid sorbents for the capture of carbon dioxide. *Int. J. Greenhouse Gas Control* **2008**, *2*, 3−8.
(58) Dawson, R.; Stockel, E.; Holst, J. R.; Adams, D. J.; Cooper, A. I. Microporous organic polymers for carbon dioxide capture. *Energy Environ. Sci.* **2011**, *4*, 4239−4245.
(59) Srinivas, G.; Krungleviciute, V.; Guo, Z. X.; Yildirim, T. Exceptional CO_2 capture in a hierarchically porous carbon with simultaneous high surface area and pore volume. *Energy Environ. Sci.* **2014**, *7*, 335−342.
(60) Yang, S.; Zhan, L.; Xu, X.; Wang, Y.; Ling, L.; Feng, X. Graphene-based porous silica sheets impregnated with polyethyleneimine for superior CO_2 Capture. *Adv. Mater.* **2013**, *25*, 2130−2134.
(61) Jordá-Beneyto, M.; Suárez-García, F.; Lozano-Castelló, D.; Cazorla-Amorós, D.; Linares-Solano, A. Hydrogen storage on chemically activated carbons and carbon nanomaterials at high pressures. *Carbon* **2007**, *45*, 293−303.
(62) Yan, Y.; Lin, X.; Yang, S.; Blake, A. J.; Dailly, A.; Champness, N. R.; Hubberstey, P.; Schroder, M. Exceptionally high H_2 storage by a metal organic polyhedral framework. *Chem. Commun.* **2009**, 1025−1027.
(63) Alam, N.; Mokaya, R. Evolution of optimal porosity for improved hydrogen storage in templated zeolite-like carbons. *Energy Environ. Sci.* **2010**, *3*, 1773−1781.
(64) Sevilla, M.; Foulston, R.; Mokaya, R. Superactivated carbide-derived carbons with high hydrogen storage capacity. *Energy Environ. Sci.* **2010**, *3*, 223−227.
(65) Sevilla, M.; Alam, N.; Mokaya, R. Enhancement of hydrogen storage capacity of zeolite-templated carbons by chemical activation. *J. Phys. Chem. C* **2010**, *114*, 11314−11319.
(66) Xia, Y.; Walker, G. S.; Grant, D. M.; Mokaya, R. Hydrogen storage in high surface area carbons: Experimental demonstration of the effects of nitrogen doping. *J. Am. Chem. Soc.* **2009**, *131*, 16493−16499.
(67) Pacula, A.; Mokaya, R. Synthesis and high hydrogen storage capacity of zeolite-like carbons nanocast using as-synthesised zeolite templates. *J. Phys. Chem. C* **2008**, *112*, 2764−2769.
(68) Yang, Z.; Xia, Y.; Sun, X.; Mokaya, R. Preparation and hydrogen storage properties of zeolite-templated carbon materials nanocast via CVD: Effect of the zeolite template and nitrogen doping. *J. Phys. Chem. B* **2006**, *110*, 18424−18431.
(69) Alam, N.; Mokaya, R. Characterisation and hydrogen storage of Pt-doped carbons templated by Pt-exchanged zeolite Y. *Microporous Mesoporous Mater.* **2011**, *142*, 716−724.
(70) Alam, N.; Mokaya, R. The effect of Al content of zeolite template on the properties and hydrogen storage capacity of zeolite templated carbons. *Microporous Mesoporous Mater.* **2011**, *144*, 140−147.
(71) Xia, Y.; Mokaya, R.; Grant, D. M.; Walker, G. S. A simplified synthesis of N-doped zeolite-templated carbons, the control of the level of zeolite-like ordering and its effect on hydrogen storage properties. *Carbon* **2011**, *49*, 844−853.
(72) Sevilla, M.; Fuertes, A. B.; Mokaya, R. Preparation and hydrogen storage capacity of highly porous activated carbon materials derived from polythiophene. *Int. J. Hydrogen Energy* **2011**, *36*, 15658−15663.
(73) Almasoudi, A.; Mokaya, R. Preparation and hydrogen storage capacity of templated and activated carbons nanocast from commercially available zeolitic imidazolate framework. *J. Mater. Chem.* **2012**, *22*, 146−152.
(74) Xia, Y.; Mokaya, R. CVD nanocasting routes to zeolite-templated carbons for hydrogen storage. *Chem. Vap. Deposition* **2010**, *16*, 322−328.
(75) Panella, B.; Hirscher, M.; Roth, S. Hydrogen adsorption in different carbon nanostructures. *Carbon* **2005**, *43*, 2209−2214.
(76) Xia, Y.; Mokaya, R. Ordered mesoporous carbon monoliths: CVD nanocasting and hydrogen storage properties. *J. Phys. Chem. C* **2007**, *111*, 10035−10039.
(77) Wang, H.; Gao, Q.; Hu, J. High hydrogen storage capacity of porous carbons prepared by using activated carbon. *J. Am. Chem. Soc.* **2009**, *131*, 7016−7022.
(78) Thomas, K. M. Hydrogen adsorption and storage on porous materials. *Catal. Today* **2007**, *120*, 389−398.
(79) Masika, E.; Mokaya, R. Hydrogen storage in high surface area carbons with identical surface areas but different pore sizes: Direct

DOI: 10.1021/acssuschemeng.5b00351
ACS Sustainable Chem. Eng. 2015, 3, 1658−1667

demonstration of the effects of pore size. *J. Phys. Chem. C* **2012**, *116*, 25734−25740.
(80) Poirier, E.; Chahine, R.; Bose, T. K. Hydrogen adsorption in carbon nanostructures. *Int. J. Hydrogen Energy* **2001**, *26*, 831−835.
(81) Gogotsi, Y.; Portet, C.; Osswald, S.; Simmons, J. M.; Yildirim, T.; Laudisio, G.; Fischer, J. E. Importance of pore size in high-pressure hydrogen storage by porous carbons. *Int. J. Hydrogen Energy* **2009**, *34*, 6314−6319.
(82) Xu, W.-C.; Takahashi, K.; Matsuo, Y.; Hattori, Y.; Kumagai, M.; Ishiyama, S.; Kaneko, K.; Iijima, S. Investigation of hydrogen storage capacity of various carbon materials. *Int. J. Hydrogen Energy* **2007**, *32*, 2504−2512.

DOI: 10.1021/acssuschemeng.5b00351
ACS Sustainable Chem. Eng. 2015, 3, 1658−1667